THE JOURNAL OF PHYSICAL CHEMISTRY C
A JOURNAL OF THE AMERICAN CHEMICAL SOCIETY

pubs.acs.org/JPCC
Article

Anharmonic Correction to the Adsorption Free Energy of Oxygen-Containing Intermediates on Pt(111) by Machine-Learned Force Field-Based Thermodynamic Integrations

Thanh-Nam Huynh, Bassim Mounssef, Jr., Dmitry I. Sharapa, Felix Studt,* and Tomáš Bučko*

Cite This: J. Phys. Chem. C 2025, 129, 16742−16755

ABSTRACT: Accurate and efficient descriptions of adsorption free energy are of fundamental importance to bringing theoretical findings closer to experiments. The present study introduced a robust combination of machine learning and (un)constrained molecular dynamics-based λ-path thermodynamic integration methods to accurately estimate the anharmonic correction to the free energy of adsorbing systems and, thus, the adsorption free energy. The approach was demonstrated for the adsorptions of the oxygenated species exhibiting different anharmonic behaviors, namely, atomic oxygen (O), hydroxyl (OH), and hydroperoxyl (OOH), on the Pt(111) surface. The corrected adsorption free energies reveal the significant influence of anharmonic effects, which could account for up to 39% of the entropy loss estimated by the conventional harmonic approximation, even at near room temperature. This highlights the limitations of the current harmonic approximation and underscores the need to account for anharmonicity for better descriptions of the adsorption processes. The present method paves the way for the accurate adsorption of free energy calculations to be performed routinely toward more powerful theoretical predictions of heterogeneously catalyzed reactions.

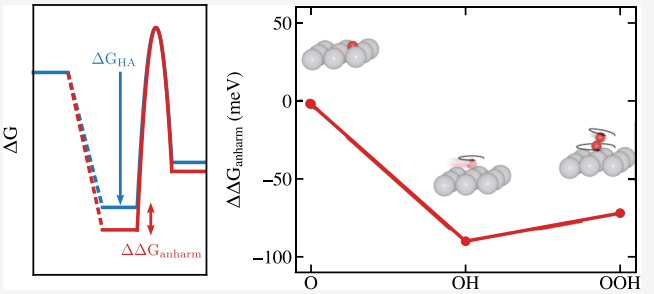

1. INTRODUCTION

The adsorption of a molecule or fragment on a surface material plays a central role in various processes in heterogeneous catalysis and surface science. The free energy of such a process is a critical indicator of the performance of catalytically active surfaces. Oftentimes, adsorption is the rate-limiting step in heterogeneously catalyzed reactions. For example, in the oxygen evolution and oxygen reduction reactions, the adsorption free energies of different oxygenated species can be used to estimate the potential at which these reactions commence.[1,2] Hence, a method for accurate calculations of the adsorption free energy is of utmost importance. Such a method would not only enhance our understanding of the catalyst systems of interest but also bolster predictive capabilities for improving catalyst designs in computational heterogeneous catalysis.

The accuracy of adsorption enthalpies has been substantially enhanced by various methods, such as using the hybrid QM:QM[3] or the RPA ensemble average.[4] On the other hand, calculating accurate entropic contribution to free energy remains challenging since it requires determining the system's partition function, which involves complete sampling of the phase space. Conventional methods employed several models to approximate the free energy (or, more accurately, the entropic contribution to free energy) by using analytically known functions to represent the partition function.[5,6] Among them, the harmonic oscillator approximation (HA)[5] has been a standard model for evaluating free energies in heterogeneous catalysis. The method assumes strong binding between adsorbates and the surface, and thus, upon adsorption, the molecule's translational and/or rotational degrees of freedom in the gas phase are converted into harmonic vibrations in the adsorbed phase. Hence, the HA partition function for the adsorbate can be straightforwardly described. This naturally introduces the term anharmonicity, defined as the deviation in the behavior of a system beyond the harmonic regime. In adsorption systems, anharmonicity stems predominantly from the translational, rotational, and/or other low-frequency modes, i.e., soft vibrational modes that are often intrinsically nonoscillatory and are therefore only poorly represented by HA. The contribution from these anharmonic motions could become considerably large, particularly at high temperatures. The failures of HA in describing free energies of adsorbed systems and the need for anharmonic correction have been extensively noted in the literature.[7−9]

Received: May 20, 2025
Revised: August 8, 2025
Accepted: August 11, 2025
Published: September 4, 2025

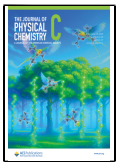

In the past decade, considerable efforts have been put into developing sophisticated approaches that can partially or fully recover the contribution from anharmonic effects and, thus, provide accurate adsorption energetics. These efforts have focused primarily on improving translational and rotational partition functions. Earlier, Sprowl et al. proposed the hindered translator (HT) and hindered rotor (HR) model, in which the adsorbate is assumed to move in two-dimensional sinusoidal potential energy surfaces (PESs) with analytic forms.[10] For this model, knowledge of the mobility of the adsorbate as a function of the thermodynamic conditions is required a priori. Several other methods have been suggested to construct the partition functions of translations (and rotations) from the explicitly sampled PESs.[11−16] Another approach was to improve the estimation of anharmonic vibrational energies by solving the 1D Schrödinger equations for the potentials of the six molecule−surface vibrations, which were directly constructed along the normal modes.[17−20] Although demonstrating improvements over the HA, these methods are still limited in describing translations (and rotations) of the adsorbate, and the anharmonic effects of the substrate are often ignored.

Alternatively, molecular dynamics (MD) calculations could be used to sample the PES and capture the complete dynamics (i.e., including anharmonicity) of the system. Quasi-harmonic approximation, based on the vibrational density of states computed from MD, was shown to improve the free energy of ethanol adsorption in the H-ZSM5 zeolite.[21] This method, even though being able to recover a part of the harmonic effects, cannot account for, for example, hindered translation.[8] Another MD-based technique is thermodynamic integration (TI),[22−24] which typically can be used to calculate the free energy difference between any two thermodynamic states. Amsler and co-workers have proposed variants of the λ-path thermodynamic integration (λ-TI) method that allowed for recovering the anharmonic contribution to the free energy of adsorption (and activation).[8,9] They demonstrated efficient samplings of the DFT PES to obtain converged adsorption free energies with a reduced computational cost by employing a suitably chosen set of internal coordinates. Despite that, for more practical systems, achieving convergences at the DFT level remains a formidable computational task. Later, Jinnouchi et al. introduced an effective approach combining machine learning (ML) and TI to calculate the free energy of adsorption and hydration.[25,26] The machine-learned force fields (MLFFs) were the efficient workhorse that realized such calculations, allowing for accurate free energy calculations. However, the choice for TI reference in this study posed convergence problems, as the phase spaces of the reference and target states, corresponding to the species in vacuum and in solution, respectively, differed significantly, making the TI implementation nontrivial. To address this problem, a more complex two-stage TI and the introduction of a model potential were invoked. For assessing the contribution of anharmonic effects to adsorption free energy, the λ-TI methods proposed by Amsler et al. are advantageous.

It is evident that the use of MLFFs, especially the one developed by Jinnouchi,[26,27] which has already been well incorporated in VASP, is promising to alleviate the computational hindrance from the sampling within the λ-TI methods. In fact, thanks to their high efficiency and accuracy, MLFFs have been increasingly used as a reliable surrogate model for free energy calculations of different systems.[25,28−30] Therefore, in the present work, we introduce MLFFs to the λ-TI workflow (hereafter referred to as the MLFF-TI workflow) to calculate the free energy of adsorptions on transition metal surfaces. The combination of cost-effective MLFFs and the well-established λ-TI method facilitates the accurate and efficient sampling of a vast majority of phase spaces at a reasonably affordable cost, which is essential for statistically reliable free energy computations. An additional supplementary adoption of the free energy perturbation (FEP) theory secures the accuracy of calculated values at the corresponding DFT level. A similar workflow employing straightforward unconstrained λ-TI has been successfully implemented to evaluate anharmonic effects in the phase transition of $SrZrS_3$.[30]

With the aid of MLFF, we demonstrate that the converged free energies could be achieved by the λ-TI calculations using the straightforward Cartesian coordinates, thus simplifying the task of choosing appropriate coordinates. Furthermore, we adopt the constrained TI method, which was originally proposed to calculate free energy barriers,[9] to handle slow convergence degrees of freedom. This comprehensive approach, together with the proliferation of MLFFs in computational heterogeneous catalysis, is promising to make free energy calculations routine.

We showcase the performance of the approach in three systems of different oxygenated species, namely, atomic oxygen (O), hydroxyl (OH), and hydroperoxyl (OOH), adsorbed on a Pt(111) surface at 300 K. These adsorption processes are essential to understanding the mechanism of heterogeneously catalytic reactions that are highly relevant to sustainable energy conversion, e.g., electrocatalytic oxygen reduction reaction (ORR) and CO oxidation,[1,31−37] although factors like hydration must also be considered as the reactions occur in aqueous media. Our findings reveal different anharmonic behaviors in these systems, indicating the inadequacy of using a single model to approximate the adsorption free energies across a reaction pathway. We further demonstrate that even at the low temperature examined, the influence of anharmonic effects in free energies of adsorption is considerable, underscoring the necessity to take these effects into account for an accurate description of the adsorption process.

2. METHODOLOGY

2.1. Machine-Learned Force Field. This work utilized the on-the-fly MLFF feature integrated into VASP in version 6.4.1. The method has been developed recently and well-adapted to various applications.[38−40] In this method, a structure data set, including structural geometries, total energies, forces, and stress tensors, is collected (on-the-fly) during a DFT MD simulation to train an MLFF. The potential energy V of a system is approximated as a sum of atomic local energies $V_i = F[\rho_i(\boldsymbol{r})]$, which are functionals of probability density $\rho_i(r)$ of finding another atom j at the position $\boldsymbol{r}$ around the atom i within its defined atomic environment. The local atomic configuration around each atom is described by Gaussian-based descriptors. These include two-body radial descriptors and three-body angular descriptors. The model utilizes Bayesian linear regression to make predictions for energies, forces, stress tensors, and the associated uncertainties in the forces for a given structure. The inclusion of uncertainties is crucial as it not only determines whether the algorithm performs additional DFT calculations and gathers more training configurations but also serves as a valuable indicator to assess whether the MLFF is extrapolating during

https://doi.org/10.1021/acs.jpcc.5c03465
J. Phys. Chem. C 2025, 129, 16742−16755

the production run. More details on the theoretical foundation of the method can be found in ref 27.

We trained separate MLFFs for different systems being investigated in the present work. Details on the training and evaluation of these MLFFs are given in Section S1 of the Supporting Information.

2.2. Machine-Learned Force Field-Aided Thermodynamic Integration (MLFF-TI). The λ-TI methods were employed to calculate the anharmonic contribution to the free energy. In the λ-TI formalism (Scheme 1), the absolute Helmholtz free energy of an anharmonic system is calculated as

Scheme 1. Relations between Various Free Energy Terms Involved in the MLFF-TI Workflow[a]

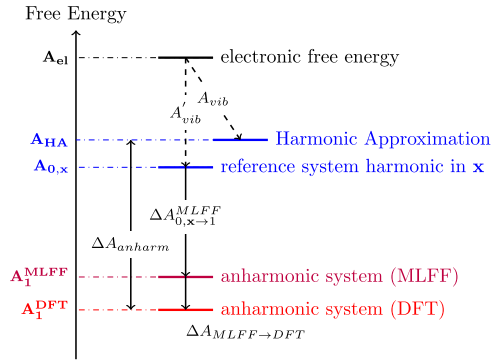

[a]The true harmonic free energy (A_{HA}) and free energy of the reference harmonic in Cartesian coordinates ($A_{0,x}$) are obtained analytically from the respective Hessian matrices.

$$A_1 = A_{0,\boldsymbol{x}} + \Delta A_{0,\boldsymbol{x}\to1} \tag{1}$$

where $A_{0,\boldsymbol{x}}$ is the free energy of an arbitrary reference system that is harmonic in Cartesian coordinates and $\Delta A_{0,\boldsymbol{x}\to1}$ is the free energy difference between the anharmonic and the harmonic reference systems, defined as

$$A_{0,\boldsymbol{x}\to1} = -k_B T \ln\left[\frac{Q_1}{Q_{0,\boldsymbol{x}}}\right] \tag{2}$$

Here, $Q_\alpha = M\int \exp(-\mathcal{H}_\alpha/k_B T)d\boldsymbol{p}d\boldsymbol{q}$ is the partition function of the system α described by the Hamiltonian $\mathcal{H}$, M is a normalization constant, T is the temperature, and k_B is the Boltzmann constant. The first term on the right-hand side of eq 1 is computed via the quasi-classical free energy expression:

$$A_{0,\boldsymbol{x}} = A_{el}(\boldsymbol{x}_0) - k_B T \sum_{i=1}^{N_{vib}} \ln \frac{k_B T}{\hbar\omega_i} \tag{3}$$

where $A_{el}(\boldsymbol{x}_0)$ is the electronic free energy for the minimum energy configuration of the reference system, N_{vib} denotes the number of vibrational modes i with real angular frequencies ω_i obtained via the finite difference method, and $\hbar$ is the reduced Planck's constant. The electronic free energy is calculated as[41]

$$A_{el}(\boldsymbol{x}_0) = -k_B T \ln\left[g_0 \exp\left(\frac{-\mathcal{V}_{0,\boldsymbol{x}}(\boldsymbol{x}_0)}{k_B T}\right)\right] \tag{4}$$

with g_0 being the spin multiplicity of the ground state. The second term of eq 1, $\Delta A_{0,\boldsymbol{x}\to1}$, can be calculated via λ-TI using straightforward unconstrained MDs as

$$\Delta A_{0,\boldsymbol{x}\to1} = \int_0^1 \langle \mathcal{V}_1 - \mathcal{V}_0\rangle_\lambda d\lambda \tag{5}$$

where λ is the coupling parameter describing the transformation path from the harmonic reference state ($\lambda = 0$) to the fully interacting state ($\lambda = 1$) and $\mathcal{V}_0$ and $\mathcal{V}_1$ are the potential energies of a configuration evaluated by harmonic and anharmonic Hamiltonians, respectively. The harmonic potential energy is computed from a harmonic force field as

$$\mathcal{V}_0(\boldsymbol{x}) = \mathcal{V}_0(\boldsymbol{x}_0) + \frac{1}{2}(\boldsymbol{x}-\boldsymbol{x}_0)^T \underline{\mathbf{H}}^{\boldsymbol{x}}(\boldsymbol{x}-\boldsymbol{x}_0) \tag{6}$$

where $\underline{\mathbf{H}}^{\boldsymbol{x}}_{ij} = \frac{\partial^2 \mathcal{V}_{0,\boldsymbol{x}}(\boldsymbol{x})}{\partial x_i \partial x_j}|_{\boldsymbol{x}=\boldsymbol{x}_0}$ is the Hessian matrix determined for an arbitrary reference $\boldsymbol{x}_0$. The V_1 is predicted by an MLFF. The $\langle\cdots\rangle_\lambda$ is the ensemble average of the quantity over the configuration space at state λ, described by the Hamiltonian

$$\mathcal{H}_\lambda = \lambda\mathcal{H}_1 + (1-\lambda)\mathcal{H}_0 \tag{7}$$

Alternatively but equivalently, constrained λ-TI[9] could be employed, which is a preferable choice for systems with convergence issues. In this method, holonomic constraints are introduced to control degrees of freedom, heavily affecting the sampling convergence. The contributions of the modes are, then, decoupled from $\Delta A_{0\to1}$:

$$\Delta A_{0,\boldsymbol{x}\to1} = \Delta A_{0\to1}(\xi') - k_B T \ln\left[\frac{P_0(\xi')}{P_1(\xi')}\right] \tag{8}$$

The term $\Delta A_{0,\boldsymbol{x}\to1}(\xi')$ is defined as the free energy difference between the harmonic reference system and the fully interacting system, with $\xi(\boldsymbol{x})$ being constrained at ξ'. This term can be computed as

$$\Delta A_{0,\boldsymbol{x}\to1}(\xi') = \int_0^1 d\lambda \frac{1}{\langle Z^{-1/2}\rangle_{\lambda,\xi'}} \langle Z^{-1/2}(\mathcal{V}_1 - \mathcal{V}_{0,\boldsymbol{x}})\rangle_{\lambda,\xi'} \tag{9}$$

where $\langle\cdots\rangle_{\lambda,\xi'}$ is the ensemble average of the quantity over the configuration space at state λ with $\xi(\boldsymbol{x}) = \xi'$and Z is the inverse mass metric tensor, defined as

$$Z = \sum_{i=1}^{N} \frac{1}{m_i} \sum_{\mu=x,y,z} \left(\frac{\partial\xi}{\partial x_{i,\mu}}\right)^2 \tag{10}$$

where m_i is the mass of atom i and μ is the Cartesian component of the position vector $\boldsymbol{x}$. The terms $P_0(\xi')$ and $P_1(\xi')$ are the probabilities of $\xi(\boldsymbol{x})$ being at ξ' in the NVT ensembles governed by the harmonic force field and MLFF, respectively. These terms can be obtained from probability density analyses of the two respective unconstrained trajectories.

Note that eq 8 can be easily generalized to multiple independent degrees of freedom:

$$\Delta A_{0,\boldsymbol{x}\to1} = \Delta A_{0\to1}(\xi_1', \xi_2', \cdots, \xi_n') - k_B T \ln \frac{P_0(\xi_1', \cdots, \xi_n')}{P_1(\xi_1', \cdots, \xi_n')} \tag{11}$$

and can serve as the basis for the approximation:

https://doi.org/10.1021/acs.jpcc.5c03465
J. Phys. Chem. C 2025, 129, 16742−16755

Scheme 2. Workflow for Computing Anharmonic Corrections via MLFF-TI in VASP[a]

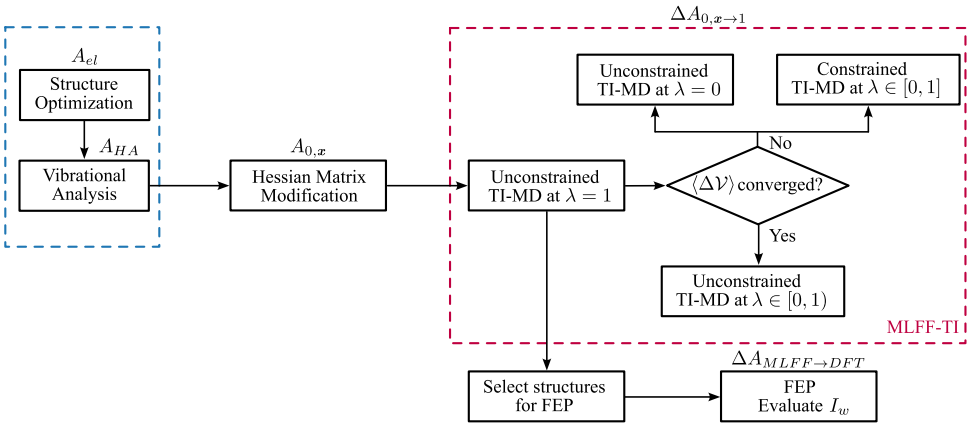

[a]The terms above some steps denote the free energy that can be computed at that stage. The blue dashed box indicates the typical steps within HA, while the red dashed box corresponds to the MLFF-aided TI procedure.

$$\Delta A_{0,\boldsymbol{x}\to 1} \approx \Delta A_{0\to 1}(\xi_1', \xi_2', \cdots, \xi_n') - k_B T \ln \frac{\prod_{i=1}^{n} P_0(\xi_i')}{\prod_{i=1}^{n} P_1(\xi_i')} = \Delta A_{0\to 1}(\xi_1', \xi_2', \cdots, \xi_n') - \sum_{i=1}^{n} k_B T \ln \frac{P_0(\xi_i')}{P_1(\xi_i')} \quad (12)$$

with n being the number of constrained degrees of freedom. We further discuss the validity of this approximation in Section S2 in the Supporting Information.

Additionally, in the MLFF-TI workflow, it is worthwhile to emphasize that the total free energy, A_1, is independent of the choice of the harmonic reference (see Section S4 in Supporting Information). As such, one could opt for either a DFT or an MLFF reference, meaning that all of the quantities relevant to the harmonic part, e.g., $A_{el}(\boldsymbol{x}_0)$, ω_i, and $\underline{\mathbf{H}}^x$, are consistently determined by the respective method.

2.3. Free Energy Perturbation. The MLFF-TI methods provide free energy values that are accurate up to the employed MLFF level. This means that the final results are influenced not only by the accuracy of MLFF in predicting individual energies and forces but also by the phase space sampled by MLFF compared with that of DFT. Therefore, different MLFFs are expected to yield various values of free energies. As a result, comparing the free energy values of different systems obtained from MLFF-TI can be prone to errors if multiple MLFFs are used. Hence, it is necessary to bring the MLFF-TI free energies to the accuracy of the DFT level on which MLFF was trained. To achieve this, the FEP[42] theory can be used to calculate the free energy difference between two methods.

The free energy difference from FEP can be computed as

$$\Delta A_{\mathrm{MLFF}\to\mathrm{DFT}} = -k_B T \ln \left\langle \exp\left(-\frac{\mathcal{V}_{\mathrm{DFT}} - \mathcal{V}_{\mathrm{MLFF}}}{k_B T} \right) \right\rangle_{\mathrm{MLFF}} \quad (13)$$

where $\mathcal{V}_{\mathrm{DFT}}$ and $\mathcal{V}_{\mathrm{MLFF}}$ are the potential energies of a given system calculated by DFT and MLFF methods, respectively, and $\langle \cdots \rangle_{\mathrm{MLFF}}$ is the ensemble average over the configurations from the MLFF trajectories. Since the MLFFs were trained on the DFT data, it is reasonable to expect that the overlaps of the configuration spaces sampled by MLFFs and DFT are significant, indicating reliable corrections from FEP.

The overlaps between MLFF's and DFT's configuration spaces are estimated by the I_w index, defined as the minimal proportion of configurations, sorted in the ascending order of potential energy difference, which collectively contribute at least 50% of the Boltzmann weight, $w_i = \exp \frac{-\Delta \mathcal{V}_i}{k_B T}$ (see details in Section S4.3).[9,43,44]

2.4. Simulation Details. Periodic DFT calculations were performed using the Vienna ab initio simulation package (VASP) code version 6.4.1.[45−48] The TI has been fully implemented in this version of VASP.[49] The Kohn−Sham equations were solved variationally in a plane-wave basis set by using the PAW method of Blöchl, as adapted by Kresse and Joubert with standard PAW potentials. The BEEF-vdW density functional[50] was employed for geometry optimizations and MD simulations using a plane-wave energy cutoff of 450 eV for all computations. A Monkhorst−Pack k-point mesh of 3 × 3 × 1 was used to sample the Brillouin zone. Convergence criteria of 10^{-6} eV and 0.001 eV Å^{-1} were applied to SCF cycles and geometry optimizations, respectively. All of the calculations were non-spin-polarized.

A 3 × 3 four-layer slab was adopted to model the Pt(111) surface. A vacuum layer of 14 Å was inserted to avoid the surface's self-interactions. The dimensions of the supercell were kept fixed for all of the calculations. Adsorption free energies were computed at a concentration of one adsorbate per unit cell (i.e., equivalent to a coverage of 1/9 ML) for the adsorbed state relative to the ideal gas state at a reference pressure of 101,325 Pa for H_2 and H_2O.

Full Hessian matrices were computed for all systems using a centered finite difference scheme. For λ-path TI, MLFF-based MD simulations were performed in the NVT ensemble at 300 K using the Andersen thermostat[51] with a collision probability of 0.05. The Andersen thermostat was chosen for its simple implementation and efficient thermal equilibration. Similar to previous studies,[8,9] hydrogen atoms were treated as tritium (m_H = 3 u). The integration step was 0.5 fs for all of the systems. The same electronic-structure-related setting was used in geometry relaxations and MD simulations.

A typical MLFF-TI workflow is presented schematically in Scheme 2. It begins with the results available for HA, namely, the optimized structure at $\boldsymbol{x}_0$ and the Hessian matrix calculated

https://doi.org/10.1021/acs.jpcc.5c03465
J. Phys. Chem. C 2025, 129, 16742−16755

Table 1. Free Energies (in eV) of the Investigated Systems at 300 K and Pressure of 101,325 Pa, Compared to the Free Energies Obtained from the Harmonic Approximation G_{HA}^{DFT}[b]

system	$G_{0,x}$	G_1^{MLFF}	G_1^{DFT}	G_{HA}^{DFT}	ΔG_{anharm}^{DFT}
H_2O[a]			−13.116	−13.116	-
H_2[a]			−7.412	−7.412	-
Pt(111)	−102.135	−102.224(0.002)	−102.222(0.002)	−102.168	−0.054(0.002)
O@Pt(111)	−106.407	−106.481(0.001)	−106.497(0.002)	−106.441	−0.056(0.002)
OH@Pt(111)	−110.412	−110.662(0.001)	−110.661(0.003)	−110.518	−0.144(0.003)
OOH@Pt(111)	−113.124	−113.366(0.001)	−113.370(0.002)	−113.244	−0.126(0.002)

[a]Harmonic oscillator/ideal gas/linear rigid rotor approximation. [b]$G_{0,x}$, free energy of the chosen harmonic reference; G_1^{MLFF}, the system's anharmonic free energy (corrected by MLFF-TI); G_1^{DFT}, the system's anharmonic free energy corrected by the FEP theory; and ΔG_{anharm}^{DFT}, anharmonic correction at the DFT level. The corresponding uncertainties are shown in the parentheses.

for that structure, which provide the values for A_{el} and A_{HA}. To define the harmonic force field in eq 6, one can either use the existing Hessian matrix or modify and transform it to improve the convergence of the TI calculations in the harmonic limit (i.e., $\lambda \rightarrow 0$). For example, the force constants (i.e., eigenvalues) can be increased to a predefined minimum eigenvalue limit if they are below that threshold. The free energy of the harmonic reference system, $A_{0,x}$, is then computed from the employed (modified) matrix $\mathbf{H}^x$. Subsequently, the free energy difference, $A_{0,x\rightarrow 1}^{MLFF}$, is calculated via either a constrained or unconstrained TI procedure. The choice can be made based on the convergence behavior of the $\langle \mathcal{V}_1 - \mathcal{V}_0 \rangle$ term for an unconstrained MD trajectory at $\lambda = 1$. If this term is well-converged, the remaining TI calculations at $\lambda < 1$ can be performed using unconstrained MD. Otherwise, the anharmonic modes are identified, and appropriate constraints are imposed to perform the TI-MD simulations. Additionally, another unconstrained MD simulation at $\lambda = 0$ is performed to obtain the necessary probability analyses for evaluating eqs 8 or 12. In the last step, a set of independent configurations is extracted from the fully interacting unconstrained trajectory (i.e., unconstrained MD trajectory at $\lambda = 1$) to perform DFT single-point calculations for FEP.

We note that, for the sake of simplicity, lattice expansion in periodic systems is neglected, allowing the Gibbs free energy (G) to be approximated by the Helmholtz free energy (A). Accordingly, all reported free energies hereafter are to be interpreted as Gibbs free energies.

3. RESULTS

In this section, we demonstrate the influence of anharmonic effects on the adsorption free energies of oxygenated adsorbates on the Pt(111) surface. Specifically, we present the anharmonic correction results obtained for four systems, namely, clean Pt, atomic oxygen at Pt (O@Pt), the hydroxyl group at Pt (OH@Pt), and the hydroperoxyl group at Pt (OOH@Pt). We then compare the corrected Gibbs free energies for these adsorptions against the results from two HA approaches to highlight the impact of anharmonicity. All results were obtained using the proposed MLFF-TI method (as introduced in the Methodology section), in which the employed MLFFs are shown to be excellent at reproducing the DFT results at the temperature of interest (see Section S1 in the Supporting Information).

3.1. Anharmonicity in the Different Systems.

3.1.1. Bare Pt(111) System. Table 1 presents the free energies (in eV) of the investigated systems at 300 K and a pressure of 101,325 Pa, compared to the free energy obtained from the harmonic approximation G_{HA}^{DFT}.

We begin our analysis by investigating the anharmonic contribution to the free energy of the bare Pt(111) surface, which, together with the gas-phase molecules, will be used as the reference for the calculations of adsorption free energies. The anharmonic effects in this system are considered to come solely from the *soft* vibrational modes of the surface atoms. These soft modes are evident by frequencies beneath 200 cm^{-1} of all surface vibrations according to DFT vibrational analysis. The system's anharmonic behaviors are illustrated in Figure 1a and b, in which the partial radial distribution functions (RDFs) for two pairs of Pt surface atoms are constructed over two 2.5 ns trajectories driven by harmonic and ML force fields. While Figure 1a shows a slight deviation of the anharmonic RDF from the harmonic counterpart for the in-plane Pt−Pt vibrational modes, a more remarkable difference is observed for the interlayer breathing mode in Figure 1b as the anharmonic distribution becomes broader with a tail extending to larger distances. These behaviors indicate that the latter breathing modes are likely the main source of the anharmonic effects on the clean Pt surface.

To account for the system's anharmonic contribution, a straightforward unconstrained λ-TI procedure using eqs 5−7 was employed using seven λ points (λ = 0.00, 0.25, 0.50, 0.75, 0.90, 0.95, and 1.00), with an MLFF MD trajectory of 2.5 ns conducted at 300 K for each point. The appropriately distributed grid and sufficiently lengthened MD simulations generate a smooth and integrable λ-path. This path consists of well-converged $\langle \Delta \mathcal{V} \rangle_\lambda$ values that decrease nonlinearly from −0.03 to −0.27 eV with an initial gradual decline and a steeper drop at the higher end of λ (Figure 1c). As expected, the associated statistical errors increase as the system transitions to more anharmonic regimes. Subsequently, the $\Delta G_{0,x\rightarrow 1}$ at the MLFF level is integrated, as per eq 5, to yield −0.089 ± 0.002 eV.

We note that the harmonic reference system here has been chosen such that all eigenvalues of the Hessian matrix lower than 1 eV $Å^{-2}$ have been increased to that limit, while the corresponding eigenvectors have been preserved (to avoid numerical instabilities at low λ, cf. Section 2.1.2, ref 8). From this modified Hessian, the vibrational harmonic free energy of the reference, $G_{0,x}$, is determined to be −102.135 eV. Considering the surface's anharmonic effects, the free energy of the system at MLFF accuracy is corrected to −102.224 ± 0.002 eV.

To attain the free energy value with a DFT accuracy, a forward FEP from MLFF to DFT is conducted. This perturbation gives a small free energy difference of 0.002 ± 0.001 eV with an I_w index as high as 0.355, indicating excellent overlap in the configuration spaces generated by the MLFF

https://doi.org/10.1021/acs.jpcc.5c03465
J. Phys. Chem. C 2025, 129, 16742−16755

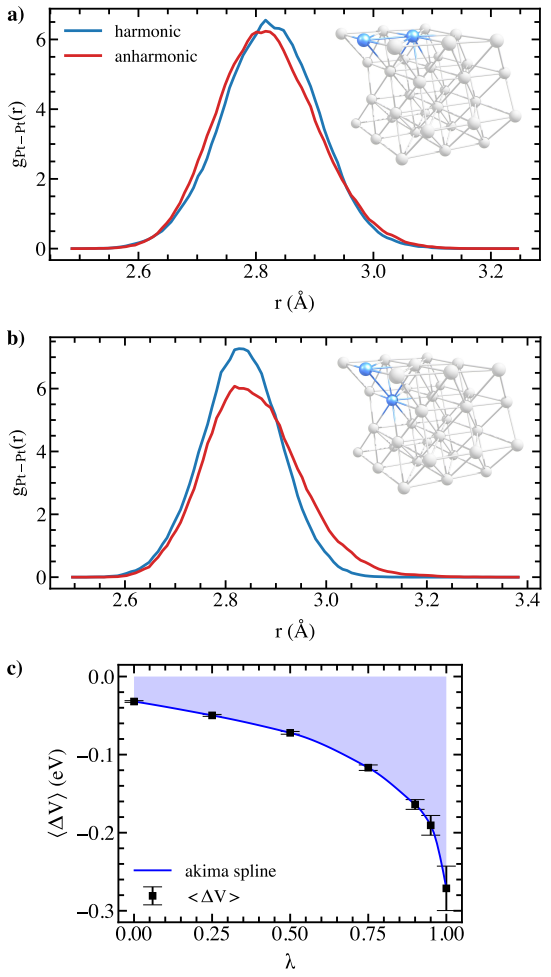

Figure 1. Anharmonic effects in a clean Pt(111) surface. Partial RDFs ($g_{Pt-Pt}(r)$) for a pair of (a) in-plane and (b) interlayer surface Pt atoms (shown as blue spheres in the insets) showing the different behaviors of the Pt surface in harmonic and anharmonic regimes. The results were computed over two corresponding 2.5 ns MD runs at 300 K driven by the potential harmonic in Cartesian coordinates and by the MLFF potential. (c) λ-Path representing the averaged energy differences for the bare Pt(111) surface system obtained from unconstrained MLFF MD runs along seven λ points at 300 K. The obtained curve is smooth and integrable, over which the integration provides the anharmonic correction $\Delta A_{0\to1}$. The blue solid curve, serving as the visual guide, represents the Akima splines connecting the computed points.

and the DFT method. We find it reasonable since the phase space of this system at 300 K is rather simple and the employed MLFF is exceptionally capable of reproducing the DFT forces and energies (see further RMSD values in forces and energies in Table S1). The final free energy at the accuracy of the DFT level G_1^{DFT} for this system arrives at −102.222 ± 0.002 eV.

Compared with a G_{HA}^{DFT} of −102.168 eV computed from the unmodified Hessian, the surface's anharmonicity decreases the free energy by as much as 54 meV, which accounts for 5% of the HA vibrational free energy.

3.1.2. O@Pt(111) System. The reference structure for the system of O adsorbing on the Pt(111) surface corresponds to the O atom sitting at an fcc hollow site, the strongest binding site, which is in agreement with the literature.[52−55] Upon adsorption, three degrees of freedom of the O adsorbate are all converted into vibrational modes with moderate frequencies (361, 363, and 415 cm^{-1}), suggesting that HA is able to describe the adsorbate's motions. Indeed, Figure 2a shows that

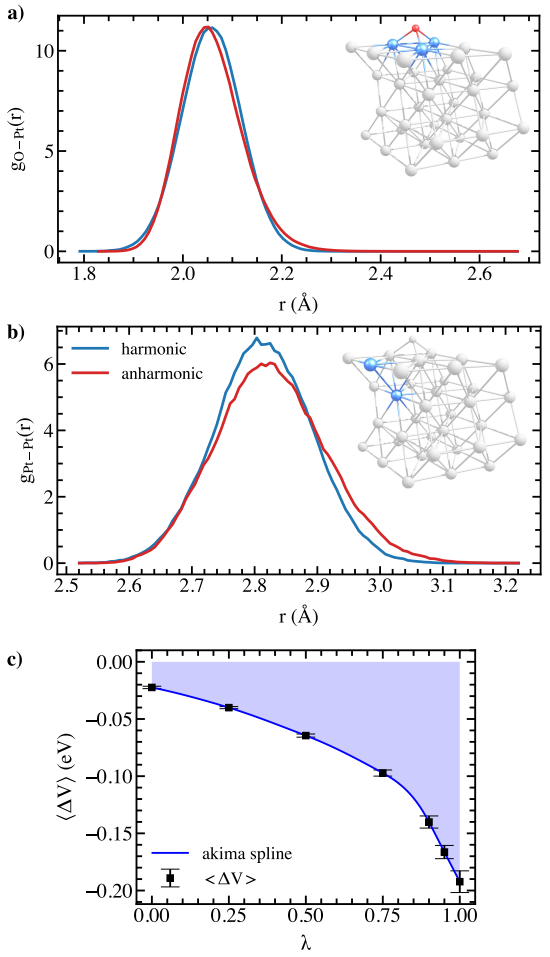

Figure 2. Anharmonic effects in the O@Pt(111) system. (a) The partial RDFs ($g_{O-Pt}(r)$ and $g_{Pt-Pt}(r)$) for the O atom and the three adjacent Pt atoms (in the inset shown as red and blue spheres, respectively) showing virtually identical behaviors of the O adsorbate on the Pt(111) surface. The results were obtained using two MD simulations with similar settings used to construct Figure 1a. (b) Partial RDFs for a pair of interlayer surface Pt atoms (as blue spheres in the inset) showing the anharmonic character of the associated breathing modes. (c) λ-Path representing averaged energy differences for the O@Pt(111) system obtained from MLFF MD runs along seven λ points at 300 K.

the behavior of the adsorbed O atom in the fully interacting regime closely mirrors the harmonic behavior, with the partial RDFs of the O−Pt distances being virtually identical for both regimes. In other words, the O adsorbate exhibits highly harmonic behavior at 300 K. On the other hand, anharmonic RDF illustrated in Figure 2b reaffirms the anharmonic effects observed for the interlayer modes of surface atoms, similar to the clean surface system. Therefore, it is expected that the anharmonic effects in this system arise primarily from surface vibrations.

Similar to the previous system, an unconstrained λ-TI procedure was employed and a readily integrable curve of $\langle \Delta \mathcal{V} \rangle_\lambda$ was obtained, as evident in Figure 2b. Analogously, due to the imposed minimum eigenvalue limit of 1 eV $Å^{-2}$ in the

https://doi.org/10.1021/acs.jpcc.5c03465
J. Phys. Chem. C 2025, 129, 16742−16755

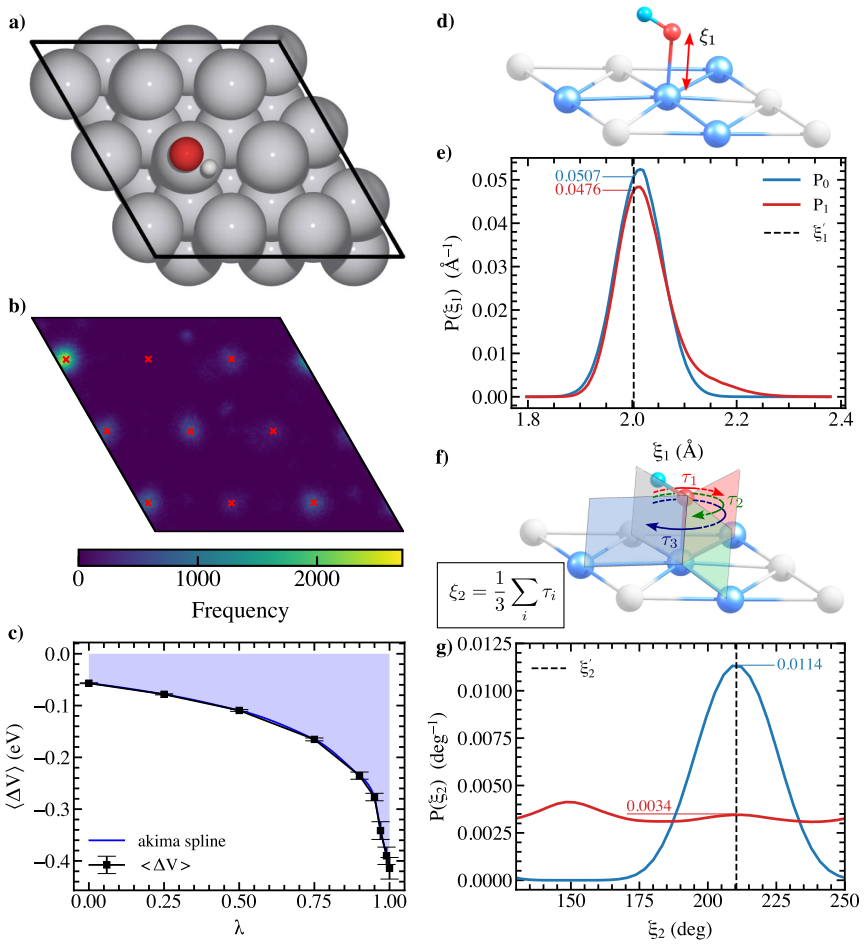

Figure 3. Anharmonic effects in the OH@Pt(111) system. (a) Reference structure for the OH@Pt(111) system. (b) Heatmap showing the mobility of the OH adsorbate on the Pt(111) surface at 300 K (red crosses depict the equilibrium positions of the topmost Pt atoms). The result is computed over 5 ns unconstrained MLFF MD trajectories. c) λ-Path representing averaged energy differences for the OH@Pt(111) system obtained from constrained MLFF MD runs along nine λ points at 300 K. (d–g) Schemes demonstrating the two constraints imposed on the OH@Pt(111) system for constrained TI calculations: the distance between the O atom and its nearest Pt atom, ξ_1, (d) and the linear combination of three torsional angles, ξ_2, (f) and their corresponding probability density distributions of ξ_1 (e) and ξ_2 (g), respectively, for the unconstrained systems driven by a harmonic force field (blue solid) and by MLFF (red solid). The dashed lines mark the positions of the reference state.

Hessian matrix, the modified harmonic reference gives a harmonic free energy contribution $G_{0,\mathscr{H}}$ of −106.407 eV, while the value for the unmodified reference G_{HA}^{DFT} is −106.441 eV. The integration over the λ-path produces a $\Delta G_{0,\mathscr{H}\to 1}$ of −0.081 ± 0.001 eV, resulting in the free energy of the system fully interacting at the MLFF level decreasing to −106.481 ± 0.001 eV.

The forward FEP provides a correction of −0.016 ± 0.001 eV, further decreasing the total free energy to −106.497 ± 0.002 eV. The larger correction for this system compared to the clean surface can be attributed to the larger RMSD in energy of the employed MLFF (0.018 eV compared to 0.010 eV; see Table S2), although the correction still falls well within the corresponding RMSD. Furthermore, it is worth emphasizing that despite the slightly larger deviation in free energies of the two levels, it is the I_w index of as large as 0.345 that guarantees reliable perturbation as it indicates the high overlap between the two phase spaces. We will demonstrate later that while such a deviation in free energies can be minimized by improving the MLFF accuracy, the final value remains unchanged given that the overlapping is significant; i.e., the I_w index is sufficiently high.

Finally, the anharmonic contribution to the free energy for this system is determined to be around −56 meV. This value, interestingly, is almost identical to that of the clean surface, confirming the source of anharmonicity as discussed above. The total anharmonic correction makes up about 6% of the free energy contributed by vibrational modes.

3.1.3. OH@Pt(111) System. Figure 3a depicts the atop binding site of the OH adsorbate on Pt(111) used as the reference structure for the TI calculations for this system. We note that there have been inconsistencies in the literature on whether the strongest binding site of OH on the Pt(111) surface is the bridge or atop site.[31,53,55] Our calculations at the BEEF-vdW level suggest that the hydroxyl species favors the atop binding position as this structure is 0.03 eV more stable than the bridge site. However, the choice of a harmonic reference should not affect the final free energy of the system.

A vibrational analysis of the OH adsorbate on the Pt surface can partly reveal its highly anharmonic nature. Of the adsorbate's six degrees of freedom, three become vibrational modes with modest to high frequencies, namely, out-of-plane hindered translation, out-of-plane hindered rotation, and OH stretching vibration at 472, 594, and 2265 cm^{-1}, respectively. However, the other in-plane degrees of freedom, including one

https://doi.org/10.1021/acs.jpcc.5c03465
J. Phys. Chem. C 2025, 129, 16742−16755

Table 2. Free Energy Components Contributing to the Free Energy Differences $\Delta G_{0,x\to 1}$ in eV Computed by the Constrained TI Method at 300 K at the MLFF Level for OH@Pt(111) and OOH@Pt(111) Systems[a]

system	$\Delta G_{0,x\to 1}(\xi')$	$-k_B T \ln \frac{P_{0,x}(\xi_i)}{P_1(\xi_i)}$		$\Delta G_{0,x\to 1}(\xi)$
		ξ_1	ξ_2	
OH@Pt	−0.132(0.001)	−0.058(0)	−0.060(0)	−0.250(0.001)
OOH@Pt	−0.144(0.001)	−0.070(0)	−0.028(0)	−0.242(0.001)

[a]The corresponding uncertainties are shown in the parentheses. See the text for the definitions of ξ_i.

hindered rotational mode and two hindered translational modes, are described by *soft* vibrational modes with respective frequencies of 59, 61, and 108 cm^{-1}. These modes, therefore, are expected to be a source of anharmonicity,[56] apart from surface motions for this system, as discussed in the previous sections.

The anharmonic characteristics of this system can be qualitatively confirmed by changes in the behavior of the OH adsorbate in the harmonic and fully interacting regimes. The OH species is strictly attached to one Pt atom corresponding to the reference structure in the trajectories driven by a harmonic force field (not shown here). Meanwhile, in the fully interacting regime, the adsorbate is highly mobile on the Pt surface at 300 K, as is evident by the heatmap of the O atom (see Figure 3b). Specifically, it frequently hops between different Pt atoms on the surface (i.e., between different degenerate minima) via bridge sites, indicating a substantial increase in the entropy. More interestingly, despite the relatively similar energies of the atop and bridge structures, as discussed previously, the bridge sites are drastically less visited. Additionally, we also observe the "helicopter"-like rotation of the OH group about the Pt−O axis (Figure 3g).

The hopping and rotations of the OH adsorbate pose a practical problem for the unconstrained TI method using the Cartesian coordinates. In particular, the large atomic deviations from the reference configuration due to these motions lead to dramatic changes in the harmonic potential energy $\mathcal{V}_{0,x}$, which, in turn, results in the very slow convergence of the $\langle \mathcal{V}_1 - \mathcal{V}_{0,x} \rangle$ term at λ close to 1. To circumvent this, we demonstrate the use of the constrained TI method, in which two holonomic constraints were imposed to eliminate the two problematic motions, and their contributions to the free energy were then captured by histogram analyses. Specifically, the adsorbate hopping was constrained by fixing the distance between the O atom and the Pt atom to which the OH species is bound ($\xi_1 = R_{O-Pt}$, Figure 3d) at the equilibrium distance of $\xi_1' = 2.002$ Å. Meanwhile, another internal coordinate, which is a symmetric linear combination of three dihedral angles formed by the OH group and surface Pt atoms ($\xi_2 = \frac{1}{3}(\tau_1 + \tau_2 + \tau_3)$) (Figure 3f) was constrained at $\xi_2' = 210.4°$ to eliminate effectively the self-rotation of the OH group. The choice of this descriptor was guided by our experience from previous TI studies for ethane hindered rotation and substitution reaction of CH_3Cl with a Cl^- anion (references 8 and 9).

MLFF MD simulations with these two coordinates constrained were conducted for nine λ points. Specifically, two additional points at 0.97 and 0.99 were included to address the steep decrease in the $\langle \Delta \mathcal{V} \rangle_\lambda$ term near the upper end. The trajectory length for these runs was 2.5 ns. Additionally, two unconstrained MLFF runs with lengths of 5 ns were carried out to determine $P(\xi_1)$ and $P(\xi_2)$.

The free energy components contributing to the free energy difference $\Delta G_{0,x\to 1}$ are summarized in Table 2. Constrained TI made it possible to achieve a λ-path over which the integration is readily performed (Figure 3c). Integrating over the obtained curve yields the free energy difference of the two constrained systems $\Delta G_{0,x\to 1}(\xi')$ of −0.132 ± 0.001 eV. As seen from Figure 3b, the OH species have visited all surface atoms and it is reasonable to assume that, at a sufficiently long time scale, the probability density of R_{O-Pt} is identical on every Pt atom on the surface. Therefore, a permutational factor of 1/9 is applied to the probability of the reference state in the fully interacting system. This implies that the probability of finding the system at $R_{O-Pt} = 2.002$ with the adsorbate bound to the central Pt atom (the reference structure) is one-ninth of the $P_1(\xi_1')$. Figure 3e shows the probability distributions of R_{O-Pt} obtained over 5 ns unconstrained MD trajectories driven by the harmonic force field and MLFF. Here, the probability density $P_1(\xi_1')$ is approximately 0.0476 $Å^{-1}$, compared to the $P_0(\xi_1')$ of 0.0507 $Å^{-1}$. The contribution from this degree of freedom is calculated at $-k_B T \ln \frac{P_0(\xi_1')}{(1/9)P_1(\xi_1')} = -0.058$ eV.

Figure 3g depicts the probability distributions of the second degree of freedom. The $P_1(\xi_2)$ distribution at the anharmonic state suggests that rotation of OH about the axis perpendicular to the surface occurs very frequently. Notably, we observe two peaks corresponding to two rotational minima that are 60° apart. While DFT predicts the minimum with $\xi_2 = 210.4°$ (the chosen reference, Figure 3a) to be 2 meV more stable, such a minimum is less visited than the other in the trajectory generated by the employed MLFF. Such a slight misassessment of the relative stability is acceptable since the energy difference is significantly smaller than the RMSD in energy of the MLFF. However, the free energy contribution from this degree of freedom should not be largely altered by this assessment and will be recovered via FEP correction. The $P_1(\xi_2')$ term is 0.0034 deg^{-1}, as compared to 0.0114 deg^{-1} of $P_0(\xi_2')$. Similar to the translational permutation, the $P_1(\xi_2')$ term is multiplied by a factor of 1/3 originating from the symmetry of the OH rotation. Therefore, the OH rotation also contributes to the free energy an amount as large as −0.060 eV. This contribution is of the same order of magnitude as the translational component.

These components add up to a $\Delta G_{0,x\to 1}$ of −0.250 ± 0.001 eV (eq 12), which is to be combined with the harmonic free energy contribution $G_{0,x}$ of −110.412 eV, which yields the total free energy G_1^{MLFF} of −110.662 ± 0.001 eV. The FEP calculation gives a negligible correction of 0.001 ± 0.002 eV, yielding the total free energy G_1^{DFT} of −110.661 ± 0.003 eV. This small FEP correction and the high associated I_w index of 0.265 indicate a large shared portion of the phase spaces sampled by MLFF and DFT and, thus, the high accuracy of the MLFF result. The anharmonic correction for this system is

https://doi.org/10.1021/acs.jpcc.5c03465
J. Phys. Chem. C 2025, 129, 16742−16755

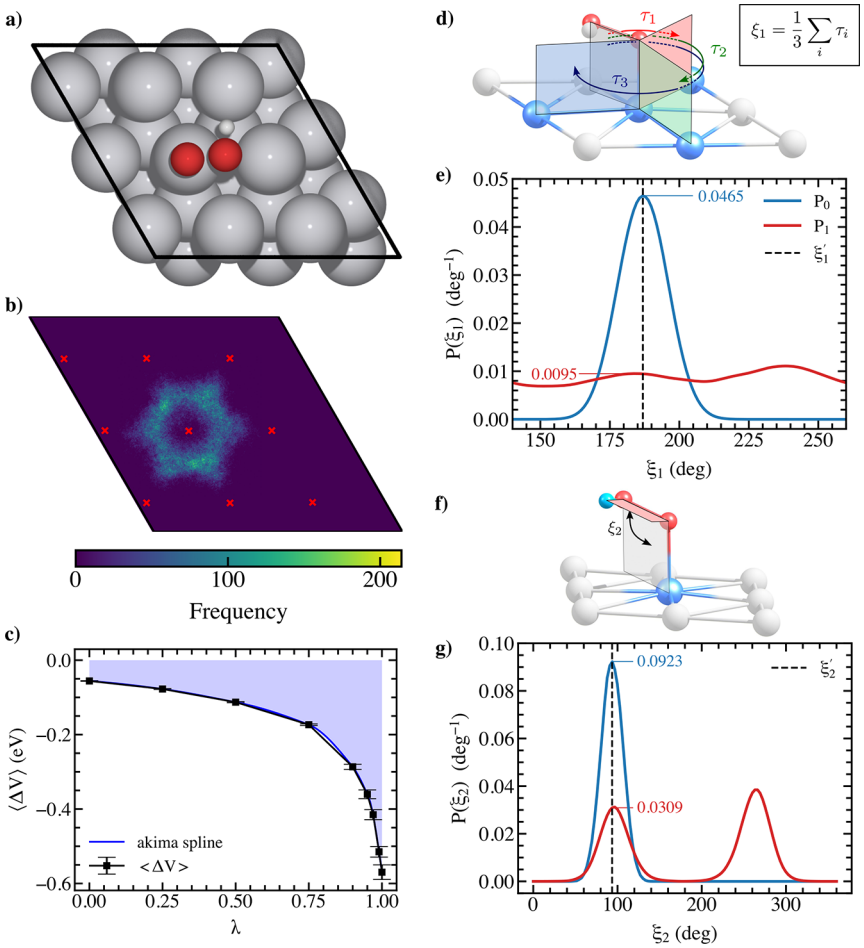

Figure 4. Anharmonic effects in the OOH@Pt(111) system. a) Reference structure for the OOH@Pt(111) system. b) Heatmap illustrating the rotation of the OOH adsorbate on the Pt(111) surface at 300 K (red crosses depict the equilibrium positions of the topmost Pt atoms). The result is computed over 5 ns unconstrained MLFF MD trajectories. c) λ-Path representing averaged energy differences for the OOH@Pt(111) system obtained from constrained MLFF MD runs along nine λ points at 300 K. (d, f) Scheme demonstrating the two constraints imposed on the OOH@Pt(111) system for constrained TI calculations. (d) Linear combination of three torsional angles (ξ_1) and (f) torsional angle of Pt−O−O-H (ξ_2). (e, g) Probability distributions of ξ_1 and ξ_2, respectively, for the unconstrained systems driven by the harmonic force field (blue solid) and by MLFF (red solid). The dashed lines mark the positions of the reference state.

calculated to be −143 meV, which makes up more than 14% of the vibrational free energy contribution estimated by HA.

3.1.4. OOH@Pt(111) System. The reference structure for the OOH@Pt(111) system corresponding to an end-on adsorption form is shown in Figure 4a. This stable structure is in good agreement with the literature.[53,57,58] Among the adsorbate's vibrational modes, only three have low frequencies. They are hindered in-plane translations at 41 and 49 cm^{-1} and a hindered in-plane rotation around an axis normal to the Pt surface through the hydrogenated atom at 103 cm^{-1}. Again, it would be reasonable to consider them highly anharmonic and likely to contribute significantly to the anharmonic correction.

An initial MLFF-MD trajectory reveals that the adsorption of the OOH species on the Pt surface is also highly anharmonic in nature. The anharmonic effects are clearly evident in the rotation of the OOH species around the Pt−O bond (as demonstrated in Figure 3b) and in a flipping motion of the OH fragment. These motions, consequently, pose difficulties for convergence due to the poor treatment of rotations in Cartesian coordinates as discussed in the previous section. Notably, we did not observe any hopping of the adsorbate along the examined trajectory; this behavior is in contrast to what could be anticipated based on the vibrational analysis.

To tackle the convergence issues, the constrained TI method has once again been shown to be advantageous. In particular, a linear combination of three torsional angles (analogous to a previous section) is used to constrain the rotation of the OOH species, while the flipping of OH is controlled by the Pt−O−O-H torsional angle. Specifically, the ξ_1 is fixed at 186.9°, whereas the ξ_2 is kept at 93.6°. These constraints are depicted in Figure 4d,f.

Similar to the OH@Pt system, we conducted the constrained TI calculations for a nine-point grid and obtained a smooth λ-path with well-converged $\langle\cdots\rangle_\lambda$ terms (Figure 4c). Integrating over the path yields a free energy difference, $\Delta G_{0,x\to1}(\xi')$, of −0.144 ± 0.001 eV. Figure 4e, g depicts the probability densities of the two rotational degrees of freedom for the harmonic and fully interacting systems, showing high anharmonic characteristics of these modes. The nearly 6-fold symmetry of the in-plane rotation of the OOH on Pt(111) is clearly shown by the two peaks of the P_1 line. This rotation is found to be even more frequent than that of OH, demonstrated in a more distributed probability density at the

https://doi.org/10.1021/acs.jpcc.5c03465
J. Phys. Chem. C 2025, 129, 16742−16755

Table 3. Comparison of the Enthalpy, Entropic Contribution, and Free Energy of Adsorptions in eV for Three Oxygenated Species on Pt(111) at 300 K Estimated by Classical HA and TI Methods[a]

	ΔH	$-T\Delta S^{HA}$	$-T\Delta S^{TI}$	ΔG^{HA}	ΔG^{TI}	$\Delta\Delta G_{anharm}$	$\Delta\Delta S$ (%)
O	1.350	0.081	0.079	1.431 (1.450)	1.429 ± 0.004	−0.002	2.7
OH	0.874	0.229	0.139	1.103 (1.118)	1.013 ± 0.005	−0.090	39.3
OOH	3.770	0.311	0.239	4.081 (4.092)	4.009 ± 0.005	−0.072	23.1

[a]Additional data from partial harmonic approximation are given in the parentheses.

fully interacting state and a low probability of the reference. Analogous to the OH rotation, a symmetry factor of 1/3 is adopted and the contribution from this degree of freedom is −0.070 eV. Additionally, the two peaks, approximately 180° apart, shown in Figure 4g evidence the rotation of the OH group about the O−O axis. The $P_1(\xi_2')$ was determined to be 0.0309 deg^{-1}, relative to $P_0(\xi_2')$ = 0.0923 deg^{-1}, which contributes −0.028 eV to the anharmonic correction. The total $\Delta G_{0,x\to 1}$ arrives at −0.242 ± 0.001 eV.

Together with the harmonic free energy contribution $\Delta G_{0,x}$ of −113.124 eV, the G_1^{MLFF} is computed to be −113.366 ± 0.001 eV. The G_1^{DFT} receives an additional −0.004 ± 0.001 eV from FEP, concluding a value of −113.370 ± 0.002 eV. The I_w index for the perturbation is as reasonably high as 0.27, ensuring the reliability of the FEP correction. The anharmonic correction for this system is −126 meV, which is more than 12% of the HA vibrational free energy contribution.

3.2. Free Energy of Adsorption and Role of Anharmonic Effects. Having obtained the accurate anharmonic free energies, we examine the influence of anharmonicity on the adsorptions of different oxygenated species on the Pt(111) surface. To evaluate their adsorption free energies, we consider the following reactions that are highly relevant for the ORR processes:

$$H_2O + Pt^* \rightarrow O^*Pt + H_2 \quad (14)$$

$$H_2O + Pt^* \rightarrow OH^*Pt + \frac{1}{2}H_2 \quad (15)$$

$$2H_2O + Pt^* \rightarrow OOH^*Pt + \frac{3}{2}H_2 \quad (16)$$

We assume the cancellation of the pV terms for the adsorbed and substrate systems; therefore, the Gibbs free energies of adsorption can be computed as follows:[8]

$$\Delta G_1 = G_{1,A@S} + aG_{0,H_2} - G_{1,S} - bG_{0,H_2O} \quad (17)$$

where $G_{1,A@S}$ and $G_{1,S}$ are the anharmonic Gibbs free energies of the adsorbed and clean surface systems, respectively, G_{0,H_2} and G_{0,H_2O} are the Gibbs free energies of the H_2 and H_2O gases, respectively, approximated by an ideal gas, rigid rotor, and harmonic oscillator model, with their associated stochiometric factors, a and b. The computed anharmonic adsorption free energies are compared to their harmonic counterparts in Table 3. Note that the anharmonic corrections to the adsorption free energy, $\Delta\Delta G_{anharm}$, arise from the difference between anharmonic corrections, ΔG_{anharm}^{DFT}, for the adsorbed and clean systems (reported in Table 1), as illustrated in Figure 5.

For the adsorption of monatomic O on Pt, the TI adsorption free energy is 1.429 ± 0.004 eV, which, within the statistical uncertainty, is identical to the full HA (FHA) value. This agreement results from the cancellation of anharmonic corrections for the adsorbed and substrate systems. There is

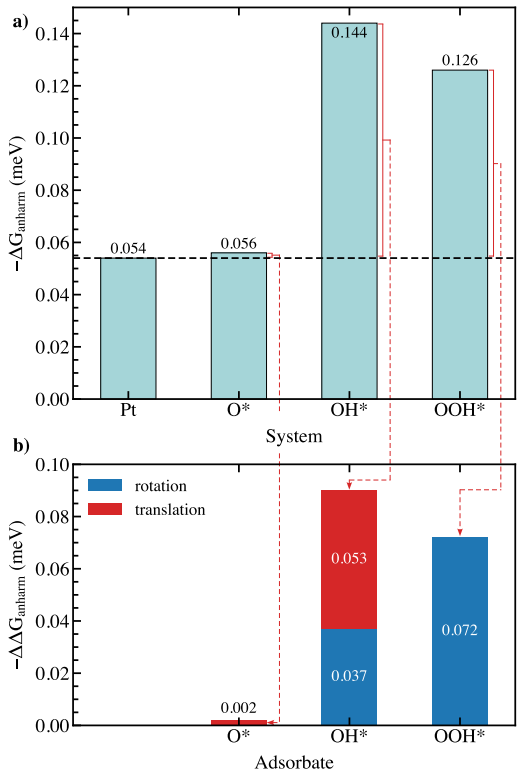

Figure 5. (a) Anharmonic corrections to the free energy of the investigated systems. (b) Resulting anharmonic corrections to the free energy of adsorption for the three adsorbates and the contributions of anharmonic modes. The black dashed horizontal line presents the anharmonic correction to the free energy of the Pt system.

a difference of −21 meV between the results of TI and partial harmonic approximation (PHA), where the surface atoms are kept frozen. This amount comes from the different contributions of surface atoms in the clean and adsorbed systems, as the difference can already be observed in FHA. This correction aligns reasonably well with the value of ∼−29 meV at 300 K as derived from Jørgensen et al.[11] for adsorption of O on Pt(111) at 0.25 ML coverage. Note that although the author solely aimed at the translational free energy of the O adsorbate, the contribution from the Pt surface atoms was implicitly captured as their positions along the z-axis were relaxed during the sampling.

The adsorption free energy obtained via TI for OH is computed to be 1.013 ± 0.005 eV. The anharmonic effects decrease the free energy by 90 and 105 meV as compared to those predicted by FHA and PHA, respectively. This significant correction is due to the higher anharmonicity in the adsorbing system, stemming from the increased entropy from the hindered translation and rotation of the adsorbate (i.e., smaller entropy loss), of which translational modes play a more important role (Figure 5b). The anharmonic correction

https://doi.org/10.1021/acs.jpcc.5c03465
J. Phys. Chem. C 2025, 129, 16742−16755

from TI is close to the correction predicted by a hindered-translator free-rotor approximation for the adsorbate (Section S6 of the Supporting Information). The increased entropy comprises up to as large as 39% of the entropic contribution to the adsorption free energy. In other words, our TI calculations recover up to more than 39% of the entropy lost upon adsorption, which is overestimated by HA.

Similarly, the Gibbs free energy of adsorption of the OOH species computed using TI is 4.009 ± 0.005 eV, which is 72 and 83 meV lower than the FHA and PHA values, respectively. As discussed, the anharmonic contribution comes from the rotation of the OOH species and the flipping motion of the OH fragment. The amount of entropy recovered for this adsorption is about 23% of the lost value estimated by HA.

4. DISCUSSION

In the present study, we have introduced the applications of the MLFF-TI workflow to correct the anharmonic contribution to the free energy of adsorption on transition metal surfaces. The investigated adsorbates demonstrate the increasing complexities in the degrees of freedom considered. We have shown that the anharmonic contribution generally correlates with the size of the adsorbates. While there is almost no anharmonic correction for the adsorption of monatomic oxygen, such a correction becomes more considerable for the cases of diatomic hydroxyl and triatomic hydroperoxyl radicals. This is because more anharmonic motions are observed with increasing sizes, e.g., translation and rotation for OH, and two (internal) rotations for OOH. Therefore, we speculate that bulky adsorbates, such as hydrocarbons and their derivatives, generally possess highly anharmonic characteristics as they involve various internal methyl rotations. As the significance of internal motions in anharmonicity increases, other analytical models, such as the HR, which considers the rotations of the entire adsorbate, become increasingly inadequate. Hence, the implementation of MLFF-TI for such cases is necessary to capture the anharmonicity and obtain the accurate free energy of adsorption.

The entropic effects of the metal surface are often neglected within the HA realm. Or more accurately, such contributions are assumed to cancel out between the adsorbed and clean surfaces. This exclusion is mainly because the vibrational modes associated with the surface have low frequencies, leading to high uncertainty in HA estimations. Many efforts to incorporate anharmonic effects also relied on this assumption. The MLFF-TI workflow enables us to accurately account for the contributions from surface atoms (see Section S4.1 in the Supporting Information) and validate such an assumption. Within the HA formalism, the inclusion of surface modes results in small decreases of 11−19 meV in adsorption free energy for the examined adsorbates (Table 3). As shown for the O's adsorption, the anharmonic contributions, which stem mainly from the surface modes, are virtually the same for the systems with and without the adsorbate. For the adsorption of OH and OOH, it is expected that the anharmonic effects of the surface atoms are slightly greater in the adsorbed systems compared to the clean surface. This is due to the surface relaxation in response to the anharmonic motions of the adsorbates, even though the deviations in positions are not significantly different from the reference configuration. Unfortunately, identifying the anharmonic contributions from different parts of the interacting system is beyond the capacity of the current MLFF-TI method and remains the subject of ongoing research. It is reasonable to conclude that the exclusion of surface modes for the investigated transition metal systems remains a valid assumption; however, it is important to acknowledge a potential discrepancy on the order of 20 meV at 300 K.

So far, we have emphasized the crucial role of anharmonic effects in the adsorption process already at a temperature as low as 300 K and the importance of considering them in free energy calculations. This requires a robust method that is suitable for routine implementations. In this context, we briefly highlight some advantages of the MLFF-TI workflow in terms of the choice of the coordinate system, harmonic reference, and the use of the FEP method to reduce systematic error in MLFF.

Conventionally, in the modeling of transition metal surfaces, it is common practice to freeze a certain number of slab bottom layers to represent the bulk. This constraint makes the use of the Cartesian harmonic potentials (eq 6) relevant because the system, as a whole, is not prone to translations and rotations. However, the adsorbate's soft motions, e.g., internal rotations and diffusion, often lead to slow convergences. It has been demonstrated that using MLFFs and imposing a few additional constraints can significantly address the issue. These constraints are typically simple internal coordinates that add minimal complexity to the coordinate system. Therefore, the choice of a coordinate set to define the harmonic potential becomes straightforward.

In the TI formalism, it has been shown that the final corrected free energy of a given system is independent of the choice of the harmonic reference configuration.[8] We reveal in Section S4.2 in the Supporting Information that the total free energy at the MLFF level, A_1^{MLFF}, depends only on the associated MLFF-predicted PES, regardless of the different references varying in the minimum limits of Hessian matrices' eigenvalues. Furthermore, we also show that the same result can be achieved when an MLFF-generated reference is used. This approach holds significant practical potential as it allows for the avoidance of optimizations and finite difference calculations at the DFT level, which is highly beneficial for large systems.

As various MLFFs produce different free energy values, the FEP method and its corresponding I_w index are the key to achieving DFT accuracy. As illustrated in Section S4.3 of the Supporting Information, thanks to the FEP, for each of the first three systems, two MLFFs trained at different regions of a system's phase space provide results with excellent agreement. Such agreements are guaranteed by the substantial overlap in phase spaces generated by these MLFFs and DFT (as observed with the high I_w values). Interestingly, these results indicate that one need not train an excessively accurate MLFF, which is relatively impractical for systems with flat PESs, in order to capture the anharmonic effects.

In short, the proposed MLFF-TI workflow offers a robust and straightforward approach to incorporate anharmonic contributions. As the MLFFs continue to gain popularity, this workflow is expected to be routinely implemented for more accurate free energy evaluations as well as better agreements with experiments.

5. CONCLUSIONS

In this article, we demonstrated the utility of the MLFF-TI workflow in calculating anharmonic corrections to the harmonic approximation of free energies of adsorption.

https://doi.org/10.1021/acs.jpcc.5c03465
J. Phys. Chem. C 2025, 129, 16742−16755

Although TI calculations are conducted mostly using the straightforward Cartesian coordinates for implementation simplicity, the intrinsic limitations of the set of coordinates in convergence are overcome, and our free energy values are obtained with negligibly small statistical uncertainties. This is partly achieved by employing the MLFFs as surrogate models, which facilitate adequate sampling of the adsorbing PESs at a readily affordable cost. Another factor that improves the statistics of our calculations is the introduction of appropriately chosen constraints to prevent slow convergence caused by problematic degrees of freedom such as hindered translation or hindered rotations. The accuracy at the DFT level of the calculated free energies is guaranteed by FEP, accompanied by the I_w index, a descriptor of the reliability of the perturbation (as well as the MLFF's quality). The MLFF-TI workflow is demonstrated to be a robust and versatile approach to accurately account for the anharmonicity of the adsorption.

We have applied the approach to study the adsorption energetics of three oxygenated species, namely, O, OH, and OOH, on the Pt(111) surface. We find that the harmonic approximation performed reasonably well to estimate the adsorption free energy of *O as the anharmonic effects originated solely from the surface's motions and can be largely canceled out. On the other hand, anharmonic effects have considerable impacts on the energetics of the other systems. The anharmonic correction to the adsorption free energy of *OH is significant, reaching −90 meV, while that of *OOH is −72 meV. These corrections, respectively, account for up to 39% and 23% of the entropy loss estimated by the harmonic approximation. The origins of anharmonicity in the two systems are also revealed to be hindered translations and rotations due to thermal excitation. As anharmonic effects have already been shown to be significantly influential at 300 K, their impact is expected to become increasingly crucial at catalytically relevant elevated temperatures. Therefore, we emphasize the necessity of incorporating the anharmonic effects in theoretical calculations for better estimations of the adsorption free energy and its derived thermodynamics and kinetics.

■ ASSOCIATED CONTENT

Data Availability Statement

All data used to support the conclusions of this work, including the references, training sets, and parameters used to train MLFF models (i.e., `ML_AB` and `INCAR` files, respectively), and TI trajectories, are openly available at dx.doi.org/10.35097/9srq4sv6cg1a0w3h.

Supporting Information

The Supporting Information is available free of charge at https://pubs.acs.org/doi/10.1021/acs.jpcc.5c03465.

Further information on the training and evaluation of MLFFs, TI technicalities, comparisons between quantum and classical harmonic approximations, comparisons with analytical approximations, and uncertainty quantification (PDF)

■ AUTHOR INFORMATION

Corresponding Authors

Felix Studt − *Institute of Catalysis Research and Technology, Karlsruhe Institute of Technology, 76344 Eggenstein-Leopoldshafen, Germany; Institute for Chemical Technology and Polymer Chemistry, Karlsruhe Institute of Technology, 76131 Karlsruhe, Germany;* orcid.org/0000-0001-6841-4232; Email: felix.studt@kit.edu

Tomáš Bučko − *Department of Physical and Theoretical Chemistry, Faculty of Natural Sciences, Comenius University Bratislava, SK-84215 Bratislava, Slovakia; Institute of Inorganic Chemistry, Slovak Academy of Sciences, SK-84236 Bratislava, Slovakia;* orcid.org/0000-0002-5847-9478; Email: bucko19@uniba.sk

Authors

Thanh-Nam Huynh − *Institute of Catalysis Research and Technology, Karlsruhe Institute of Technology, 76344 Eggenstein-Leopoldshafen, Germany;* orcid.org/0000-0003-4740-4347

Bassim Mounssef, Jr. − *Institute of Catalysis Research and Technology, Karlsruhe Institute of Technology, 76344 Eggenstein-Leopoldshafen, Germany*

Dmitry I. Sharapa − *Institute of Catalysis Research and Technology, Karlsruhe Institute of Technology, 76344 Eggenstein-Leopoldshafen, Germany;* orcid.org/0000-0001-9510-9081

Complete contact information is available at: https://pubs.acs.org/10.1021/acs.jpcc.5c03465

Notes

The authors declare no competing financial interest.

■ ACKNOWLEDGMENTS

T.N.H gratefully acknowledges support by GRK 2450. This work was primarily performed on the HoReKa supercomputer funded by the Ministry of Science, Research and the Arts Baden-Württemberg and by the Federal Ministry of Education and Research. Additionally, the authors acknowledge support from the state of Baden-Württemberg through bwHPC and the German Research Foundation (DFG) through grant no. INST 40/575-1 FUGG (JUSTUS 2 cluster, RVs bw17D011). D.I.S and F.S also acknowledge financial support from the German Research Foundation (DFG)(FOR 5715, HyPerCat, project-ID 525028514, project TP8 (STU 703/10-1)). Financial support from the Helmholtz Association, Germany, is also gratefully acknowledged. T.B. acknowledges support from the Slovak Research and Development Agency under Contract No. APVV-20-0127 and the grant VEGA 1/0254/24 from the Ministry of Education Research, Development and Youth of the Slovak Republic.

■ REFERENCES

(1) Nørskov, J. K.; Rossmeisl, J.; Logadottir, A.; Lindqvist, L.; Kitchin, J. R.; Bligaard, T.; Jónsson, H. Origin of the Overpotential for Oxygen Reduction at a Fuel-Cell Cathode. *J. Phys. Chem. B* **2004**, *108*, 17886−17892.

(2) Rossmeisl, J.; Logadottir, A.; Nørskov, J. K. Electrolysis of water on (oxidized) metal surfaces. *Chem. Phys.* **2005**, *319*, 178−184.

(3) Svelle, S.; Tuma, C.; Rozanska, X.; Kerber, T.; Sauer, J. Quantum Chemical Modeling of Zeolite-Catalyzed Methylation Reactions: Toward Chemical Accuracy for Barriers. *J. Am. Chem. Soc.* **2009**, *131*, 816−825.

(4) Chehaibou, B.; Badawi, M.; Bučko, T.; Bazhirov, T.; Rocca, D. Computing RPA Adsorption Enthalpies by Machine Learning Thermodynamic Perturbation Theory. *J. Chem. Theory Comput.* **2019**, *15*, 6333−6342.

(5) Gokhale, A. A.; Kandoi, S.; Greeley, J. P.; Mavrikakis, M.; Dumesic, J. A. Molecular-level descriptions of surface chemistry in

kinetic models using density functional theory. *Chem. Eng. Sci.* **2004**, *59*, 4679−4691.
(6) Campbell, C. T.; Sprowl, L. H.; Árnadóttir, L. Equilibrium Constants and Rate Constants for Adsorbates: Two-Dimensional (2D) Ideal Gas, 2D Ideal Lattice Gas, and Ideal Hindered Translator Models. *J. Phys. Chem. C* **2016**, *120*, 10283−10297.
(7) Collinge, G.; Yuk, S. F.; Nguyen, M.-T.; Lee, M.-S.; Glezakou, V.-A.; Rousseau, R. Effect of Collective Dynamics and Anharmonicity on Entropy in Heterogenous Catalysis: Building the Case for Advanced Molecular Simulations. *ACS Catal.* **2020**, *10*, 9236−9260.
(8) Amsler, J.; Plessow, P. N.; Studt, F.; Bučko, T. Anharmonic Correction to Adsorption Free Energy from DFT-Based MD Using Thermodynamic Integration. *J. Chem. Theory Comput.* **2021**, *17*, 1155−1169.
(9) Amsler, J.; Plessow, P. N.; Studt, F.; Bučko, T. Anharmonic Correction to Free Energy Barriers from DFT-Based Molecular Dynamics Using Constrained Thermodynamic Integration. *J. Chem. Theory Comput.* **2023**, *19*, 2455−2468.
(10) Sprowl, L. H.; Campbell, C. T.; Árnadóttir, L. Hindered Translator and Hindered Rotor Models for Adsorbates: Partition Functions and Entropies. *J. Phys. Chem. C* **2016**, *120*, 9719−9731.
(11) Jørgensen, M.; Grönbeck, H. Adsorbate Entropies with Complete Potential Energy Sampling in Microkinetic Modeling. *J. Phys. Chem. C* **2017**, *121*, 7199−7207.
(12) Jørgensen, M.; Chen, L.; Grönbeck, H. Monte Carlo Potential Energy Sampling for Molecular Entropy in Zeolites. *J. Phys. Chem. C* **2018**, *122*, 20351−20357.
(13) Bajpai, A.; Mehta, P.; Frey, K.; Lehmer, A. M.; Schneider, W. F. Benchmark First-Principles Calculations of Adsorbate Free Energies. *ACS Catal.* **2018**, *8*, 1945−1954.
(14) Waitt, C.; Miles, A. R.; Schneider, W. F. Adsorbate Free Energies from DFT-Derived Translational Energy Landscapes. *J. Phys. Chem. C* **2021**, *125*, 20331−20342.
(15) Blöndal, K.; Sargsyan, K.; Bross, D. H.; Ruscic, B.; Goldsmith, C. F. Adsorbate Partition Functions via Phase Space Integration: Quantifying the Effect of Translational Anharmonicity on Thermodynamic Properties. *J. Phys. Chem. C* **2021**, *125*, 20249−20260.
(16) Blöndal, K.; Sargsyan, K.; Bross, D. H.; Ruscic, B.; Goldsmith, C. F. Configuration Space Integration for Adsorbate Partition Functions: The Effect of Anharmonicity on the Thermophysical Properties of CO−Pt(111) and CH_3OH−Cu(111). *ACS Catal.* **2023**, *13*, 19−32.
(17) Piccini, G.; Sauer, J. Quantum Chemical Free Energies: Structure Optimization and Vibrational Frequencies in Normal Modes. *J. Chem. Theory Comput.* **2013**, *9*, 5038−5045.
(18) Piccini, G.; Sauer, J. Effect of Anharmonicity on Adsorption Thermodynamics. *J. Chem. Theory Comput.* **2014**, *10*, 2479−2487.
(19) Galimberti, D. R.; Sauer, J. Chemically Accurate Vibrational Free Energies of Adsorption from Density Functional Theory Molecular Dynamics: Alkanes in Zeolites. *J. Chem. Theory Comput.* **2021**, *17*, 5849−5862.
(20) Rybicki, M.; Sauer, J. Rigid Body Approximation for the Anharmonic Description of Molecule−Surface Vibrations. *J. Chem. Theory Comput.* **2022**, *18*, 5618−5635.
(21) Alexopoulos, K.; Lee, M.-S.; Liu, Y.; Zhi, Y.; Liu, Y.; Reyniers, M.-F.; Marin, G. B.; Glezakou, V.-A.; Rousseau, R.; Lercher, J. A. Anharmonicity and Confinement in Zeolites: Structure, Spectroscopy, and Adsorption Free Energy of Ethanol in H-ZSM-5. *J. Phys. Chem. C* **2016**, *120*, 7172−7182.
(22) Chipot, C.; Pohorille, A.; Castleman, A. W.; Toennies, J. P.; Yamanouchi, K.; Zinth, W., Eds. *Free Energy Calculations: Theory and Applications in Chemistry and Biology*; Springer Series in CHEMICAL PHYSICS; Springer: Berlin, Heidelberg, 2007; Vol. *86*.
(23) Straatsma, T. P.; Berendsen, H. J. C. Free energy of ionic hydration: Analysis of a thermodynamic integration technique to evaluate free energy differences by molecular dynamics simulations. *J. Chem. Phys.* **1988**, *89*, 5876−5886.
(24) de Oliveira, C. A. F.; Hamelberg, D.; McCammon, J. A. Coupling Accelerated Molecular Dynamics Methods with Thermodynamic Integration Simulations. *J. Chem. Theory Comput.* **2008**, *4*, 1516−1525.
(25) Jinnouchi, R.; Karsai, F.; Kresse, G. Making free-energy calculations routine: Combining first principles with machine learning. *Phys. Rev. B* **2020**, *101*, No. 060201(R).
(26) Jinnouchi, R.; Karsai, F.; Verdi, C.; Kresse, G. First-principles hydration free energies of oxygenated species at water−platinum interfaces. *J. Chem. Phys.* **2021**, *154*, No. 094107.
(27) Jinnouchi, R.; Karsai, F.; Kresse, G. On-the-fly machine learning force field generation: Application to melting points. *Phys. Rev. B* **2019**, *100*, No. 014105.
(28) Grabowski, B.; Ikeda, Y.; Srinivasan, P.; Körmann, F.; Freysoldt, C.; Duff, A. I.; Shapeev, A.; Neugebauer, J. Ab initio vibrational free energies including anharmonicity for multicomponent alloys. *npj Comput. Mater.* **2019**, *5*, 80.
(29) Cheng, B.; Engel, E. A.; Behler, J.; Dellago, C.; Ceriotti, M. Ab initio thermodynamics of liquid and solid water. *Proc. Natl. Acad. Sci. U. S. A.* **2019**, *116*, 1110−1115.
(30) Jaykhedkar, N.; Bystrický, R.; Sýkora, M.; Bučko, T. Investigating the role of dispersion corrections and anharmonic effects on the phase transition in SrZrS3: A systematic analysis from AIMD free energy calculations. *J. Chem. Phys.* **2024**, *160*, No. 014710.
(31) Panchenko, A.; Koper, M. T. M.; Shubina, T. E.; Mitchell, S. J.; Roduner, E. Ab Initio Calculations of Intermediates of Oxygen Reduction on Low-Index Platinum Surfaces. *J. Electrochem. Soc.* **2004**, *151*, A2016.
(32) Hyman, M. P.; Medlin, J. W. Mechanistic Study of the Electrochemical Oxygen Reduction Reaction on Pt(111) Using Density Functional Theory. *J. Phys. Chem. B* **2006**, *110*, 15338−15344.
(33) Qi, L.; Yu, J.; Li, J. Coverage dependence and hydroperoxyl-mediated pathway of catalytic water formation on Pt (111) surface. *J. Chem. Phys.* **2006**, *125*, No. 054701.
(34) Wasileski, S. A.; Janik, M. J. A first-principles study of molecular oxygen dissociation at an electrode surface: a comparison of potential variation and coadsorption effects. *Phys. Chem. Chem. Phys.* **2008**, *10*, 3613.
(35) Janik, M. J.; Taylor, C. D.; Neurock, M. First-Principles Analysis of the Initial Electroreduction Steps of Oxygen over Pt(111). *J. Electrochem. Soc.* **2009**, *156*, B126.
(36) Duan, Z.; Wang, G. A first principles study of oxygen reduction reaction on a Pt(111) surface modified by a subsurface transition metal M (M = Ni, Co, or Fe). *Phys. Chem. Chem. Phys.* **2011**, *13*, 20178.
(37) van Spronsen, M. A.; Frenken, J. W. M.; Groot, I. M. N. Surface science under reaction conditions: CO oxidation on Pt and Pd model catalysts. *Chem. Soc. Rev.* **2017**, *46*, 4347−4374.
(38) Bokdam, M.; Lahnsteiner, J.; Sarma, D. D. Exploring Librational Pathways with on-the-Fly Machine-Learning Force Fields: Methylammonium Molecules in $MAPbX_3$ (X = I, Br, Cl) Perovskites. *J. Phys. Chem. C* **2021**, *125*, 21077−21086.
(39) Jaykhedkar, N.; Bystrický, R.; Sýkora, M.; Bučko, T. Understanding the structure-band gap relationship in SrZrS 3 at elevated temperatures: a detailed NPT MD study. *Journal of Materials Chemistry C* **2022**, *10*, 12032−12042.
(40) Berger, E.; Lv, Z.-P.; Komsa, H.-P. Raman spectra of 2D titanium carbide MXene from machine-learning force field molecular dynamics. *Journal of Materials Chemistry C* **2023**, *11*, 1311−1319.
(41) Jensen, F. *Introduction to Computational Chemistry*; 2nd ed.; John Wiley & Sons: Nashville, TN, 2007.
(42) Zwanzig, R. W. High-Temperature Equation of State by a Perturbation Method. I. Nonpolar Gases. *J. Chem. Phys.* **1954**, *22*, 1420−1426.
(43) Bučko, T.; Gešvandtnerová, M.; Rocca, D. Ab Initio Calculations of Free Energy of Activation at Multiple Electronic Structure Levels Made Affordable: An Effective Combination of Perturbation Theory and Machine Learning. *J. Chem. Theory Comput.* **2020**, *16*, 6049−6060.

(44) Herzog, B.; Chagas Da Silva, M.; Casier, B.; Badawi, M.; Pascale, F.; Bučko, T.; Lebègue, S.; Rocca, D. Assessing the Accuracy of Machine Learning Thermodynamic Perturbation Theory: Density Functional Theory and Beyond. *J. Chem. Theory Comput.* **2022**, *18*, 1382−1394.
(45) Kresse, G.; Hafner, J. Ab initio molecular dynamics for liquid metals. *Phys. Rev. B* **1993**, *47*, 558−561.
(46) Kresse, G.; Hafner, J. Ab initio molecular-dynamics simulation of the liquid-metal−amorphous-semiconductor transition in germanium. *Phys. Rev. B* **1994**, *49*, 14251−14269.
(47) Kresse, G.; Furthmüller, J. Efficiency of ab-initio total energy calculations for metals and semiconductors using a plane-wave basis set. *Comput. Mater. Sci.* **1996**, *6*, 15−50.
(48) Kresse, G.; Furthmüller, J. Efficient iterative schemes for ab initio total-energy calculations using a plane-wave basis set. *Phys. Rev. B* **1996**, *54*, 11169−11186.
(49) VASP Wiki *Thermodynamic Integration*, 2025, https://www.vasp.at/wiki/index.php/Thermodynamic_integration, accessed 24-07-2025.
(50) Wellendorff, J.; Lundgaard, K. T.; Møgelhøj, A.; Petzold, V.; Landis, D. D.; Nørskov, J. K.; Bligaard, T.; Jacobsen, K. W. Density functionals for surface science: Exchange-correlation model development with Bayesian error estimation. *Phys. Rev. B* **2012**, *85*, No. 235149.
(51) Andersen, H. C. Molecular dynamics simulations at constant pressure and/or temperature. *J. Chem. Phys.* **1980**, *72*, 2384−2393.
(52) Getman, R. B.; Xu, Y.; Schneider, W. F. Thermodynamics of Environment-Dependent Oxygen Chemisorption on Pt(111). *J. Phys. Chem. C* **2008**, *112*, 9559−9572.
(53) de Morais, R. F.; Franco, A. A.; Sautet, P.; Loffreda, D. Coverage-dependent thermodynamic analysis of the formation of water and hydrogen peroxide on a platinum model catalyst. *Phys. Chem. Chem. Phys.* **2015**, *17*, 11392−11400.
(54) Malek, A.; Eikerling, M. H. Chemisorbed Oxygen at Pt(111): a DFT Study of Structural and Electronic Surface Properties. *Electrocatalysis* **2018**, *9*, 370−379.
(55) Gray, C. M.; Saravanan, K.; Wang, G.; Keith, J. A. Quantifying solvation energies at solid/liquid interfaces using continuum solvation methods. *Mol. Simul.* **2017**, *43*, 420−427.
(56) Blöndal, K.; Badger, K.; Sargsyan, K.; Bross, D. H.; Ruscic, B.; Goldsmith, C. F. Importance sampling within configuration space integration for adsorbate thermophysical properties: a case study for CH3/Ni(111). *Phys. Chem. Chem. Phys.* **2024**, *26*, 17265−17273.
(57) Ford, D. C.; Nilekar, A. U.; Xu, Y.; Mavrikakis, M. Partial and complete reduction of O2 by hydrogen on transition metal surfaces. *Surf. Sci.* **2010**, *604*, 1565−1575.
(58) Cahyanto, W. T.; Escaño, M. C.; Kasai, H.; Arevalo, R. L. Pt(111)-Alloy Surfaces for Non-Activated OOH Dissociation. *e-Journal of Surface Science and Nanotechnology* **2011**, *9*, 352−356.

https://doi.org/10.1021/acs.jpcc.5c03465
J. Phys. Chem. C 2025, 129, 16742−16755